JACS
JOURNAL OF THE AMERICAN CHEMICAL SOCIETY
pubs.acs.org/JACS
Article

Locking Effect in Metal@MOF with Superior Stability for Highly Chemoselective Catalysis

Yicheng Zhong,[†] Peisen Liao,[†] Jiawei Kang, Qinglin Liu, Shihan Wang, Suisheng Li, Xianlong Liu, and Guangqin Li*

Cite This: *J. Am. Chem. Soc.* 2023, 145, 4659−4666
Read Online
ACCESS | Metrics & More | Article Recommendations | Supporting Information

ABSTRACT: Ultrasmall metal nanoparticles (NPs) show high catalytic activity in heterogeneous catalysis but are prone to reunion and loss during the catalytic process, resulting in low chemoselectivity and poor efficiency. Herein, a locking effect strategy is proposed to synthesize high-loading and ultrafine metal NPs in metal−organic frameworks (MOFs) for efficient chemoselective catalysis with high stability. Briefly, the MOF ZIF-90 with aldehyde groups cooperating with diamine chains via aldimine condensation was interlocked, which was employed to confine *in situ* formation of Au NPs, denoted as Au@L-ZIF-90. The optimized Au@L_a-ZIF-90 has highly dispersed Au NPs (2.60 ± 0.81 nm) with a loading amount around 22 wt % and shows a great performance toward 3-aminophenylacetylene (3-APA) from the selective hydrogenation of 3-nitrophenylacetylene (3-NPA) with a high yield (99%) and excellent durability (over 20 cycles), far superior to contrast catalysts without chains locking and other reported catalysts. In addition, experimental characterization and systematic density functional theory calculations further demonstrate that the locked MOF modulates the charge of Au nanoparticles, making them highly specific for nitro group hydrogenation to obtain 3-APA with high selectivity (99%). Furthermore, this locking effect strategy is also applicable to other metal nanoparticles confined in a variety of MOFs, and all of these catalysts locked with chains show great selectivity (≥90%) of 3-APA. The proposed strategy in this work provides a novel and universal method for precise control of the inherent activity of accessible metal nanoparticles with a programmable MOF microenvironment toward highly specific catalysis.

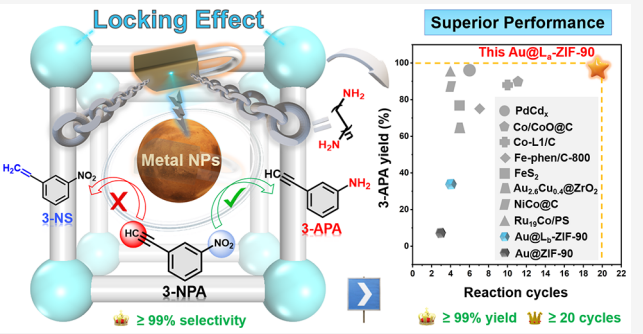

INTRODUCTION

Chemoselective hydrogenation is an important process in chemical industries, including medicine, perfume, and petrochemicals.[1−5] Specifically, 3-aminophenylacetylene (3-APA), obtained from the selective hydrogenation of the nitro group in 3-nitrophenylacetylene (3-NPA), is a vital intermediate in the production of the antitumor agent Erlotinib and fluorescent labels.[6−10] However, conventional catalysts usually tend to hydrogenate the alkynyl group of 3-NPA rather than the nitro group, as the alkynyl group is more favorable in thermodynamics.[11] Therefore, it is a great challenge to design catalysts with highly selective hydrogenation of the nitro group rather than the alkynyl group.

Metal nanoparticle (MNP) catalysts, such as Au, with excellent hydrogenation capacity, have received an enormous amount of research interest for decades.[12−17] To date, ultrafine metal nanoparticles (UMNPs) with a uniform size distribution have opened up new avenues in heterogeneous catalysis, profiting from their high surface-to-volume ratio and large active site density,[18−23] but obtaining the desirable material still remains challenging because the aggregation of MNPs often occurs, especially with a high loading amount.[24] Moreover, metal nanoparticles are easy to lose in the harsh catalytic conditions, leading to an undesired decrease in catalytic activity.[25,26] Thus, to obtain specific catalysts with ultrasmall and high-loading MNPs, simultaneously having a suitable electronic structure state for chemoselective catalysis, is still a difficult issue.

Metal−organic framework (MOF) materials with clear and tunable structures are an ideal model platform to design catalysts at the molecular level.[27−36] In particular, the incorporation of metal nanoparticles (MNPs) in MOFs has been rapidly developed in the field of heterogeneous catalysis.[37−42] The nanosized pores of MOFs with unique and confined interactions[43−50] are beneficial for synthesizing UMNPs. Moreover, amines and imines have been used as stabilizing agents for the fabrication of UMNPs during

Received: November 26, 2022
Published: February 15, 2023

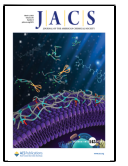

https://doi.org/10.1021/jacs.2c12590
J. Am. Chem. Soc. 2023, 145, 4659−4666

nucleation and surface growth.[51−55] We envision the preparation of ultrasmall and high-loading nanoparticles by modifying the MOF with long chains via aldimine condensation and growing the nanoparticles *in situ*, so that the particles are firmly locked in the MOF. Furthermore, the electronic valence states of UMNPs can be regulated by the MOF microenvironment to realize specific catalytic reactions.

Herein, we propose a locking effect strategy to synthesize high-loading UMNPs in MOFs for boosting chemoselective catalysis. An imine-modified MOF ZIF-90 named L_a-ZIF-90 with a locking effect was prepared and employed to modulate the loaded Au NPs. The as-formed Au@L_a-ZIF-90 has highly dispersed Au NPs with a loading amount of about 22 wt %, a high yield (99%) and excellent reusability (over 20 cycles) of 3-APA from selective hydrogenation of 3-NPA, outperforming those contrast catalysts without a locked structure. Further characterization and systematic density functional theory (DFT) calculations disclose that the locking effect could create ultrasmall, high-loading Au NPs with high structural stability and modulate the energy barriers in the hydrogenation steps on the nitro and alkynyl groups, thus enhancing the desirable 3-APA yield. Importantly, this strategy is universal to synthesize other metal NPs in MOFs.

RESULTS AND DISCUSSION

The preparation of locked MOFs is illustrated in Figure 1. First, ZIF-90, assembled from Zn ions and imidazole-2-carboxaldehyde (ICA), was selected as the mainframe with exposed aldehyde groups. Then different diamines (L_x, x = 4, 5, 6, 8, or 12, where x is the number of carbon chains in diamines) were linked to ZIF-90 by an imine condensation reaction. Typically, diaminobutane (L_4), diaminopentane (L_5), and hexanediamine (L_6), with molecule sizes between 6 and 9 nm, were chosen as mixed linkers (named as L_a) in a certain molar ratio to react with ZIF-90 for the synthesis of L_a-ZIF-90 via aldimine condensation according to the distances of different aldehyde groups (Figure S1). As shown in the Fourier transformation infrared (FTIR) spectrum (Figure S2a), the bond at 1676 cm^{-1} in the spectra is attributed to the C═O stretching frequency of ZIF-90. After the aldimine condensation with L_a, the bond at 1633 cm^{-1} attributed to C═N of the imine group was observed;[56] meanwhile, the intensity of the C═O stretching frequency at 1676 cm^{-1} of corresponding sample decreased, indicating that the aldimine condensation was successful. In contrast, the single chain (L_4, L_5, or L_6) and longer mixed chains (L_8+L_{12}, denoted as L_b) did not have a satisfactory condensation yield because an abundance of aldehyde groups still existed, as shown in the FTIR spectrum (Figure S2a,c). Powder X-ray diffraction (XRD) patterns show that the structure of ZIF-90 could be maintained after modification of the chains (Figure S2b,d). Au NPs were further loaded onto L_a-ZIF-90 through *in situ* growth using $KAuCl_4$ and further reduced by $NaBH_4$; the final material is denoted as Au@L_a-ZIF-90.

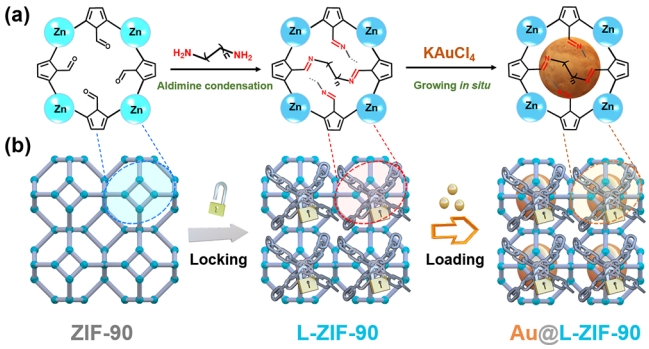

Figure 1. (a) Schematic representation for the association of imine bonds with linkers by an aldimine condensation reaction and *in situ* growth of Au NPs. (b) Synthesis process of Au@L-ZIF-90.

In order to clearly characterize the structure of the obtained material, XRD was carried out. Au (111 plane) and ZIF-90 diffractions were detected in Au@L_a-ZIF-90 according to the XRD results (Figure S2b),[57,58] which suggest that Au NPs are successfully loaded and the framework of ZIF-90 is maintained. As shown in the scanning electron microscopy (SEM) and transmission electron microscopy (TEM) images (Figure 2a,b and Figure S3a), Au nanoparticles are well dispersed in the MOF without any aggregation, with a size of 2.60 ± 0.81 nm. The high-resolution transmission electron microscopy (HRTEM) image further shows lattice fringes of the nanoparticles at 0.24 nm (Figure 2c), which corresponds to the Au(111) plane.[59,60] The high-angle annular dark-field scanning transmission electron microscopy (HAADF-STEM) image (Figure 2d) and energy-dispersive spectroscopy (EDS) elemental mappings were further performed to verify the existence and dispersity of Au NPs, as the homogeneous distribution of Au, Zn, C, N, and O was observed in Au@L_a-ZIF-90 (Figure 2e,f and Figure S4). On the other hand, it can be found that the Au@L_b-ZIF-90 with longer chains shows a little larger size (4.46 ± 1.38 nm, Figure S3b) of Au NPs compared to that with Au@L_a-ZIF-90. However, Au@ZIF-90 without any locking chains displays a large Au size and poor dispersion (6.36 ± 1.65 nm, Figure S3c). The Au loading amount of Au@L_a-ZIF-90 is about 22 wt % based on the inductively coupled plasma optical emission spectroscopy (ICP-OES) result (Table S1). Hence, a material with high Au loading content, ultrasmall nanoparticles, and uniform distribution is successfully prepared simultaneously through chains locked in the MOF, which is superior to other reported Au@MOF materials synthesized by traditional methods, as summarized in Table S2. To understand the effect of different diamines on the growth of metal nanoparticles, nitrogen gas

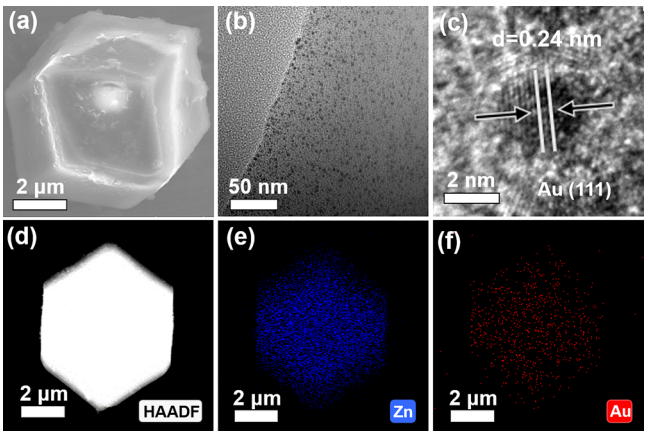

Figure 2. Morphology characterization of Au@L_a-ZIF-90 for (a) SEM image, (b) TEM image, (c) HRTEM image, and (d) HAADF-STEM image. (e,f) EDS elemental mapping data and corresponding Zn and Au elements in the selected region of Au@L_a-ZIF-90.

https://doi.org/10.1021/jacs.2c12590
J. Am. Chem. Soc. 2023, 145, 4659−4666

adsorption at 77 K was carried out. As shown in Figure S5, the pore distributions curves of ZIF-90, L_b-ZIF-90, and L_a-ZIF-90 are similar, which indicates that the microporous nature was maintained after the introduction of diamine linkers. The observed slight decrease in surface area may be due to the smaller pore aperture of L_a-ZIF-90 and L_b-ZIF-90 relative to that of ZIF-90, which prevents access to the pores by N_2 molecules,[61] leading to smaller Brunauer−Emmett−Teller surface areas. Moreover, the shorter chains locking L_a-ZIF-90 provide smaller space for the Au NPs to grow, resulting in Au nanoparticles much smaller than L_b-ZIF-90 and ZIF-90.

To investigate the structural stability of Au@L_a-ZIF-90, Au@L_b-ZIF-90, and Au@ZIF-90, the three materials were treated in hot water at 80 °C for 2 days. With the protection of chains, the basic framework of Au@L_a-ZIF-90 can be maintained, as evidenced by FTIR and XRD results (Figure S6a,b). For the unlocked ZIF-90 and Au@L_b-ZIF-90 with less locking effect, the frames completely collapsed after treatment for just 24 h, with the disappearance of MOF diffraction peaks in the XRD patterns. Moreover, the UV−vis result (Figure S6c) displays a relatively strong absorption peak of ICA at 288 nm that appeared in the filtered mother liquor of Au@ZIF-90, while for Au@L_a-ZIF-90, the peak is much lower. These above experiments fully demonstrate the role of the locking effect for improving the superior durability of MOFs.

Hydrogenation of Nitrophenylacetylene. Considering the excellent performance of gold nanoparticles in the selective hydrogenation and Lewis alkaline environment of imine groups onto L_a-ZIF-90,[62] the obtained material Au@L_a-ZIF-90 with high loading and ultrafine metal nanoparticles may be efficient for the selective hydrogenation of the nitro group to the amino group for nitroarenes, specifically in the presence of C≡C bonds. First, selective hydrogenation of 3-NPA was investigated as a model reaction to explore the optimized catalytic reaction conditions, and the reaction path is shown in Figure 3a. Based on the optimization (Table S3), the subsequent hydrogenation of 3-NPA was performed with a catalyst in MeOH solvent at room temperature. As the reaction progressed, Au@L_a-ZIF-90 showed a strong ability to produce 3-APA with 99% conversion and 99% selectivity within 5 min (Figure 3b and Figure S7). For Au@L_b-ZIF-90, the conversion is 46% and selectivity is 72%, and the undesired byproduct, 3-nitrophenylacetylene (3-NS, 23% selectivity), is produced. For Au@ZIF-90, the conversion of 3-NPA and 3-APA selectivity is relatively low (11% conversion of 3-NPA, 50% selectivity of 3-APA, and 43% selectivity of 3-NS).

To confirm the catalytic sites, ZIF-90 and L_a-ZIF-90 as catalysts were further analyzed for comparison, negligible product (~0.5%) was detected as shown in Table S3, thus the catalytic activity comes from Au nanoparticles. The commercial Au/C catalyst (14.6 wt % Au) was also tested under the same condition but only showed a low selectivity of 60.5% for 3-APA, which indicates that the microenvironment of the locked MOF is beneficial for high selectivity toward the hydrogenation of nitroarenes. Furthermore, Au@L_a-ZIF-90 with lower amounts of Au (theoretical load capacity: 5, 10, and 15%) were also synthesized as catalysts for 3-APA generation (Figures S8 and S9). As displayed in Figure S8, the higher Au-loading catalyst shows higher conversion in 5 min, which highlights the superiority of the catalyst with high-loading Au NPs.

Stability. Moreover, cycle experiments were performed to test the reusability of catalysts. As expected, there was no

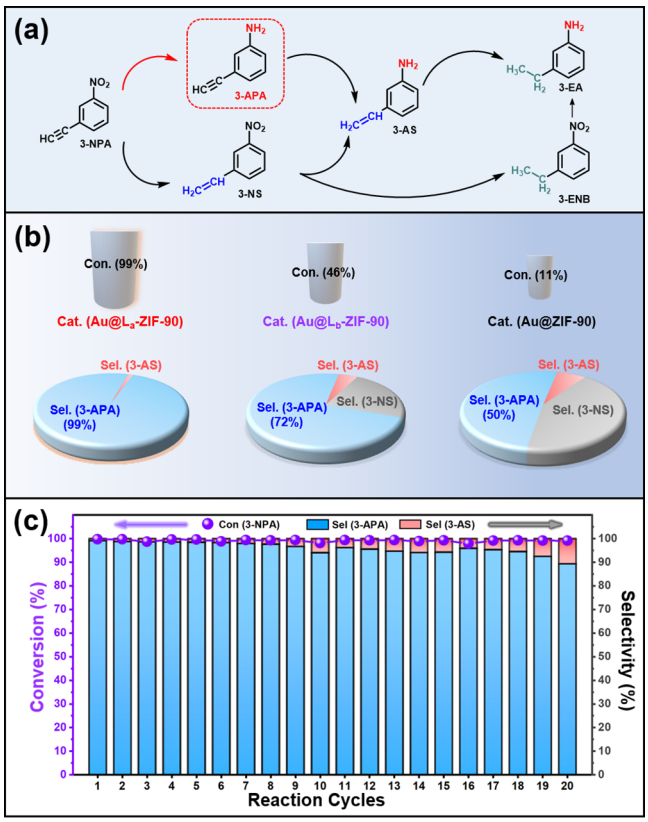

Figure 3. (a) Illustration of the total reaction paths of 3-NPA hydrogenation; (b) 3-NPA selective hydrogenation performances carried on Au@L_a-ZIF-90, Au@L_b-ZIF-90, and Au@ZIF-90; (c) recyclability experiment results carried out on Au@L_a-ZIF-90.

significant decrease even after 20 consecutive cycles for Au@L_a-ZIF-90 in the 3-APA production reaction, indicating the good stability and intrinsic reusability of Au@L_a-ZIF-90 (Figure 3c). The stability of Au@L_a-ZIF-90 after catalytic reactions (20 cycles) was established by TEM first to characterize the size change of the catalyst after cycling. As shown in Figure S10a, no significant agglomeration is observed in the TEM images of Au@L_a-ZIF-90, and the size of the Au nanoparticles is 3.56 ± 1.03 nm, just a little bit bigger than the fresh one. According to XRD structural characterization and FTIR results (Figure S11), it can be found that the framework of Au@L_a-ZIF-90 is still maintained and the crystallinity is almost the same as that of the fresh one, indicating its outstanding stability. In contrast, the catalytic performance of Au@L_b-ZIF-90 and Au@ZIF-90 changes significantly after just four or three cycles (Figure S12). For Au@L_b-ZIF-90 and Au@ZIF-90 after cycles test, Au nanoparticles change to larger sizes of 5.55 ± 1.58 and 7.08 ± 2.06 nm, respectively (Figure S10b,c). As shown in Figure S11, the decrease of crystallinity is obvious for Au@L_b-ZIF-90 and Au@ZIF-90, especially for the latter, which has no locking effect of chains. Moreover, the decrease of the C═O stretching frequency bond at 1676 cm^{-1} in the FTIR spectra of Au@L_b-ZIF-90 and Au@ZIF-90 indicates the loss of imidazole-2-carboxaldehyde in the structure of ZIF-90.

Filtration experiments were performed to detect whether there was structural damage and loss of active components resulting in abnormal performances of these catalysts. As shown in Figure S13, the three catalysts were removed by filtration after 2 min. The results show that there was no

https://doi.org/10.1021/jacs.2c12590
J. Am. Chem. Soc. 2023, 145, 4659−4666

catalytic activity after filtration of Au@L_a-ZIF-90, while the filtrate after removing Au@L_b-ZIF-90 and Au@ZIF-90 obviously continued working. Therefore, it is speculated that their structures have changed and are accompanied by the loss of Au active species. As revealed by ICP-OES and contrast tests (Tables S4 and S5), the active species may be the ultrasmall Au nanoparticles which come from the dissolved Au species from Au@L_b-ZIF-90 and Au@ZIF-90 during reaction and are reformed with the assistance of $NaBH_4$.

Furthermore, as listed in Table S6, the Au and Zn weight percentages in the recovered catalyst Au@L_a-ZIF-90 were determined to be similar to that of the fresh one. Au@L_a-ZIF-90 presents the best catalytic performance compared with other reported catalysts for NPA selective hydrogenation to APA, as summarized in Table S7, which highlights the advantages of the locking effect. Therefore, the locking effect of chains in the MOF not only prevents the loss and agglomeration of Au nanoparticles but also improves the stability of the frame, leading to long-term and excellent catalytic activity.

Mechanism. To verify the influence of the locking effect on Au NPs toward 3-NPA selective hydrogenation, X-ray photoelectron spectroscopy (XPS) measurement was performed to explore the electronic structure of Au@L_a-ZIF-90. Figure 4a,b shows that the Au $4f_{7/2}$ peak of Au@L_a-ZIF-90

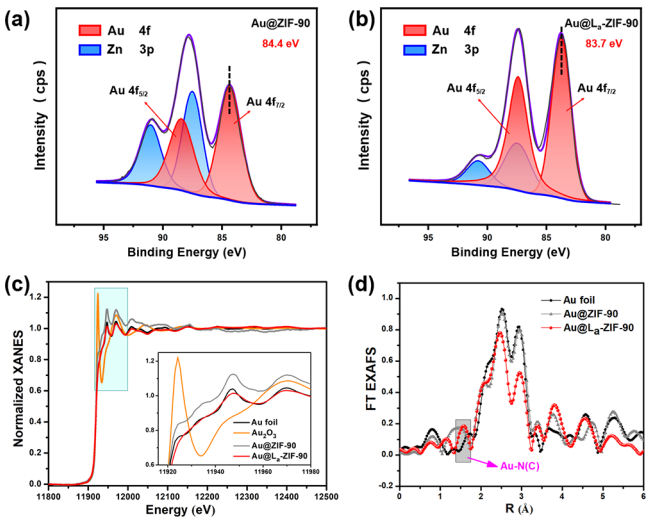

Figure 4. XPS spectra of Au 4f for (a) Au@ZIF-90, (b) Au@L_a-ZIF-90, (c) normalized Au L_3-edge XANES spectra,and (d) FT k_2-weighted EXAFS spectra of samples.

shifts to a lower binding energy (83.7 eV) compared with Au@ZIF-90 (84.4 eV), indicating that charge transfer from the imine chains to Au NPs exists. The Au $4f_{7/2}$ peak of Au@L_b-ZIF-90 is located at 84.2 eV (Figure S14), which is somewhere between Au@ZIF-90 and Au@L_a-ZIF-90, further verifying that the electronic state of Au NPs is related to the chain linkers. Moreover, N 1s and C 1s spectra of imine in Au@L_a-ZIF-90 shift to a higher binding energy (Figures S15 and S16) relatively to L_a-ZIF-90, and minimal changes of Au@ZIF-90 in the XPS spectra of Zn 2p and O 1s are observed compared to that with ZIF-90 (Figures S17 and S18), indicating there is a negligible interaction between Au NPs and ZIF-90. Thus, it can be concluded that the charge transfer occurs from the locking chains. The above results indicate that the Au electronic states are effectively regulated by chain locking in Au@L_a-ZIF-90 and Au@L_b-ZIF-90 via electron transfer from imine bonds to Au NPs. The chemical state of Au NPs in recycled Au@L_a-ZIF-90 after 20 runs is well-maintained but changes evidently in Au@ZIF-90 and Au@L_b-ZIF-90, which further proved the superior stability of Au@L_a-ZIF-90 (Figures S19−S23). To further analyze the electronic structures, the normalized X-ray absorption near-edge structure (XANES) were performed. As shown in the Au L_3-edge XANES spectra (Figure 4c), Au@L_a-ZIF-90 has lower energy of the adsorption edge (E_0) than Au foil and Au@ZIF-90, suggesting the electron richness of Au NPs, which is in accordance with the XPS result. Simultaneously, the Fourier transform extended X-ray absorption fine structure (EXAFS) spectrum of Au@L_a-ZIF-90 presents main peaks at 1.8−3.3 Å belonging to Au−Au bonding, which is the same as that on Au@ZIF-90 and Au foil (Figure 4d), while Au@L_a-ZIF-90 demonstrates a strong Au-ligand peak located around 1.7 Å, which can be attributed to Au−N(C) bonds.[63−66] Besides, the Fourier transform EXAFS spectrum of Zn and the normalized XANES spectra at the Zn K-edge in Au@L_a-ZIF-90 are in substantial agreement with those of Au@ZIF-90 (Figure S24), indicating the alike coordination modes of Zn. The results of XPS and X-ray absorption structure (XAS) fully demonstrate the regulation of electron-rich states of Au species arising from the locking effect. Considering the electron status of MNP catalysts related to hydrogenation of the nitro group[67−70] and combining the catalytic activity by the locking effect presented above, we speculate that the binding energy of Au 4f is related to the catalytic performance, and the negative Au NPs may contribute to higher selective activity.

Having confirmed that the Au NPs are the catalytic sites and the 3-APA yield increases with the increase of electron density of Au, we hypothesized that the locking effect may regulate the electronic state of Au and the selectivity of 3-APA. Then ZIF-65-CF_3 with an electron-withdrawing ability was used as a platform to obtain no locking positive Au NPs, named Au@ZIF-65-CF_3 (Figure S25). The XPS analysis (Figure S25b) proves that Au NPs are electron-deficient as the Au $4f_{7/2}$ peaks located at 84.5 eV are higher compared to that of metallic Au (84.3 eV).[71,72] The summarized hydrogenation results show that no locking Au@ZIF-65-CF_3 loaded with positive Au NPs tends to hydrogenate the alkynyl group to the main product of trivial 3-NS; however, Au@L_a-ZIF-90 with negative Au NPs tends to selectively hydrogenate the nitro group to valuable 3-APA (Figure S26).

Bearing the above experimental results in mind, DFT calculations were carried out on locked Au(111) and unlocked Au(111) surfaces with negative and positive charges that presented the most exposed facets of the Au NPs according to the XRD patterns and HRTEM images, and the models as presented in Figure S27 were constructed. The thermochemistry hydrogenation energy barriers of different reaction pathways were calculated to understand the selective hydrogenation of 3-NPA (Figure 5), and the corresponding optimized intermediates are shown in Figures S28 and S29. Specifically, the hydrogenation processes could potentially occur on both nitro and alkynyl groups in the first step. Over the locked Au surface, the energy barriers for hydrogenation on the nitro group and alkynyl group are 0.14 and 0.59 eV, respectively (Figure 5a), indicating that the hydrogenation process of the nitro group was favorable kinetically in path 1 rather than path 2. Then the following steps were all exothermic reactions that happen spontaneously in the

https://doi.org/10.1021/jacs.2c12590
J. Am. Chem. Soc. 2023, 145, 4659−4666

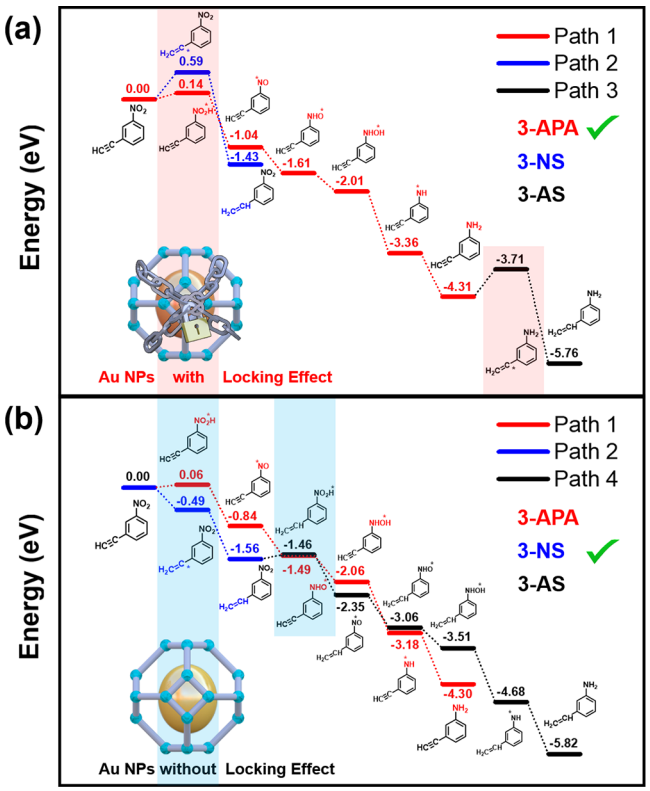

Figure 5. Gibbs free energy variation along the reaction coordinate of hydrogenation of 3-NPA on (a) locked negatively charged Au(111) model and (b) unlocked positively charged Au(111) model.

second-sixth of path 1, until forming 3-APA. It can be found that the path 3 reaction requires climbing over a barrier higher than 0.60 eV, which is difficult to trigger subsequent hydrogenation reactions on the alkynyl group of 3-APA to form 3-AS. Hence, 3-APA is the favorable target product in the hydrogenation steps over chain-locked Au NPs. In sharp contrast, the alkynyl group is the favorable target in the first hydrogenation step over the unlocked Au surface, judging from the energy barriers for hydrogenation on the alkynyl group and the nitro group, which were −0.49 and 0.06 eV, respectively (Figure 5b). After two hydrogenation steps of path 2, 3-NS was formed. In addition, in the next step, which was the first hydrogenation step in path 4, was endothermic. The energy barrier is 0.10 eV, higher than 0.06 eV of first step in path 1. Hence, evidently, the unlocked Au NPs prefer to hydrogenate the alkynyl group to 3-NS as the dominant product. The above results further elucidate that the locking effect on Au NPs can reverse the energy barriers of the reaction steps to selectively hydrogenate the nitro group rather than the alkynyl group in thermodynamics, leading enhanced 3-APA selectivity. In other words, the locking effect strategy not only promotes preparation of high-loading ultrafine Au NPs in MOFs with excellent stability but also regulates the reaction path toward highly selective hydrogenation of the nitro group.

Universality. To generalize this outstanding locking effect in catalysis, Au@L_a-ZIF-90 was evaluated in the hydrogenation of a wide range of nitroarenes containing diverse substituent groups, as shown in Table 1. For most of the nitro derivatives, 99% selectivity and high yield are achieved. Overall, this catalyst with a locking effect has good universality toward nitroarene hydrogenation catalytic performance.

Table 1. Au@L_a-ZIF-90-Catalyzed Hydrogenation of Nitro Substrates[a]

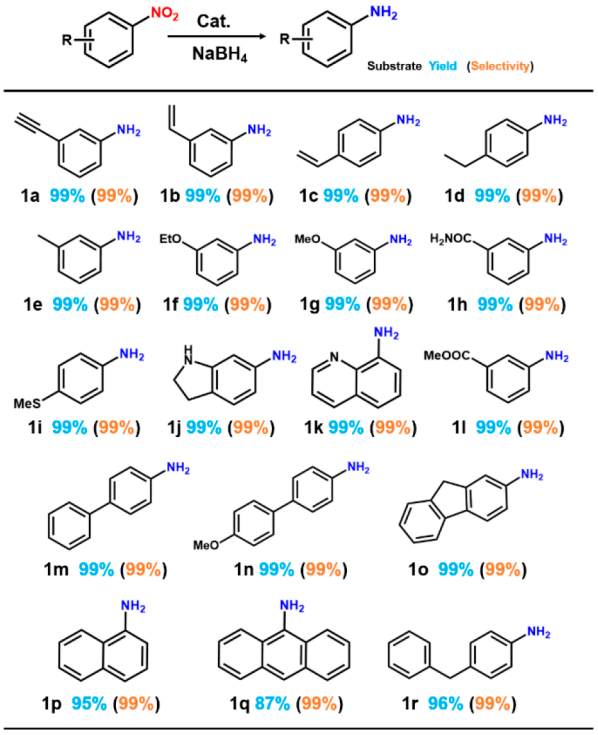

[a]Reaction conditions: substrate (0.5 mmol) except 1q (0.125 mmol) due to the solubleness, catalyst (1 mol % of metal), methanol (5 mL), 4 equiv of $NaBH_4$, 25 °C, 5 min reaction time.

In the research of 3-APA production (Table S7), the catalysts with good performance are mainly composed of noble metals such as Pt, Ru, and Pd. It is necessary to develop cheaper and useful metal species to reduce the costs. Inspiringly, our outstanding locking effect strategy can be easily expanded to other metal systems. For instance, Ag, Co, and Cu, such relatively cheap metals, were chosen to load into L_a-ZIF-90 and used as catalysts (Figures S30−S33 and Table S8), which all show a far superior 3-APA selectivity (over 92%) compared to that of M@ZIF-90 (M = Ag, Co, and Cu) without a locking effect.

Of special note, this locking effect strategy can be extended to other MOF systems, like the extensive UiO-66-NH_2, which reacted with dialdehydes (butanedial, glutaraldehyde, and adipaldehyde, denoted as L_c) to form a MOF with a locking effect (Figure S34a), further loading Au *in situ*, named as Au@L_c-UiO-66 (Figure S34b). The hydrogenation results show Au@L_c-UiO-66 also has excellent yield (90%) of 3-APA, better than that of Au@UiO-66-NH_2 without a locking effect (Figure S34c). These results bode well for designing appropriate microenvironments of MOFs with a locking effect to achieve desired products.

CONCLUSION

In general, we propose a locking effect strategy to synthesize high-loading ultrafine MNPs in chain-locked MOFs via aldimine condensation, which has been applied in selective nitroarene hydrogenation. Specifically, Au@L_a-ZIF-90 with a locking effect showed a high yield (99%) of 3-APA from the selective hydrogenation of 3-NPA and excellent durability (over 20 cycles). According to catalytic results and detailed

https://doi.org/10.1021/jacs.2c12590
J. Am. Chem. Soc. 2023, 145, 4659−4666

characterization, the outstanding activity is attributed to high-loading ultrafine Au NPs firmly stabilized in the MOF homogeneously and the modulation of an electron state of Au species arising from the locking effect, which could make negatively charged Au NPs prone to hydrogenate the nitro group, thus promoting highly selective catalytic performance. Furthermore, although 3-NS is thermodynamically favorable compared with 3-APA, DFT calculations demonstrate that for locked Au NPs, the energy barriers for forming 3-APA are lower than those for 3-NS but not enough to get over the barrier of excessive hydrogenation product 3-AS, resulting in high 3-APA yield during the selective hydrogenation process. Moreover, this strategy is universal to synthesize other metal NPs in various MOFs. The proposed locking effect strategy is a promising avenue to controllably fabricate stable high-loading UMNPs via an engineered microenvironment with locked framework materials to achieve desired catalytic products.

■ ASSOCIATED CONTENT

Supporting Information

The Supporting Information is available free of charge at https://pubs.acs.org/doi/10.1021/jacs.2c12590.

Experimental methods and supporting figures (PDF)

■ AUTHOR INFORMATION

Corresponding Author

Guangqin Li − *MOE Laboratory of Bioinorganic and Synthetic Chemistry, Lehn Institute of Functional Materials, School of Chemistry, Sun Yat-Sen University, Guangzhou 510275, P.R. China;* orcid.org/0000-0002-1233-5591; Email: liguangqin@mail.sysu.edu.cn

Authors

Yicheng Zhong − *MOE Laboratory of Bioinorganic and Synthetic Chemistry, Lehn Institute of Functional Materials, School of Chemistry, Sun Yat-Sen University, Guangzhou 510275, P.R. China*

Peisen Liao − *MOE Laboratory of Bioinorganic and Synthetic Chemistry, Lehn Institute of Functional Materials, School of Chemistry, Sun Yat-Sen University, Guangzhou 510275, P.R. China*

Jiawei Kang − *MOE Laboratory of Bioinorganic and Synthetic Chemistry, Lehn Institute of Functional Materials, School of Chemistry, Sun Yat-Sen University, Guangzhou 510275, P.R. China*

Qinglin Liu − *MOE Laboratory of Bioinorganic and Synthetic Chemistry, Lehn Institute of Functional Materials, School of Chemistry, Sun Yat-Sen University, Guangzhou 510275, P.R. China*

Shihan Wang − *MOE Laboratory of Bioinorganic and Synthetic Chemistry, Lehn Institute of Functional Materials, School of Chemistry, Sun Yat-Sen University, Guangzhou 510275, P.R. China*

Suisheng Li − *MOE Laboratory of Bioinorganic and Synthetic Chemistry, Lehn Institute of Functional Materials, School of Chemistry, Sun Yat-Sen University, Guangzhou 510275, P.R. China*

Xianlong Liu − *MOE Laboratory of Bioinorganic and Synthetic Chemistry, Lehn Institute of Functional Materials, School of Chemistry, Sun Yat-Sen University, Guangzhou 510275, P.R. China*

Complete contact information is available at: https://pubs.acs.org/10.1021/jacs.2c12590

Author Contributions

†Y.Z. and P.L. contributed equally.

Notes

The authors declare no competing financial interest.

■ ACKNOWLEDGMENTS

This work was supported by NSFC Projects (22075321, 21821003, and 21890380), the Program for Guangdong Introducing Innovative and Entrepreneurial Teams (2017ZT07C069), and the Overseas High-level Talents Plan of China.

■ REFERENCES

(1) Lou, S.; Luo, G.; Yamaguchi, S.; An, K.; Nishiura, M.; Hou, Z. Modular Access to Spiro-dihydroquinolines *via* Scandium-Catalyzed Dearomative Annulation of Quinolines with Alkynes. *J. Am. Chem. Soc.* **2021**, *143*, 20462−20471.

(2) Wang, L.; Guan, E.; Zhang, J.; Yang, J.; Zhu, Y.; Han, Y.; Yang, M.; Cen, C.; Fu, G.; Gates, B. C.; Xiao, F.-S. Single-site catalyst promoters accelerate metal-catalyzed nitroarene hydrogenation. *Nat. Commun.* **2018**, *9*, 1362.

(3) Zhang, S.; Chang, C.-R.; Huang, Z.-Q.; Li, J.; Wu, Z.; Ma, Y.; Zhang, Z.; Wang, Y.; Qu, Y. High Catalytic Activity and Chemoselectivity of Sub-nanometric Pd Clusters on Porous Nanorods of CeO_2 for Hydrogenation of Nitroarenes. *J. Am. Chem. Soc.* **2016**, *138*, 2629−2637.

(4) Wei, J.; Zhao, L.; He, C.; Zheng, S.; Reek, J. N. H.; Duan, C. Metal-Organic Capsules with NADH Mimics as Switchable Selectivity Regulators for Photocatalytic Transfer Hydrogenation. *J. Am. Chem. Soc.* **2019**, *141*, 12707−12716.

(5) Pang, S. H.; Schoenbaum, C. A.; Schwartz, D. K.; Medlin, J. W. Directing Reaction Pathways by Catalyst Active-Site Selection using Self-Assembled Monolayers. *Nat. Commun.* **2013**, *4*, 2448.

(6) Deng, X.; Qin, B.; Liu, R.; Qin, X.; Dai, W.; Wu, G.; Guan, N.; Ma, D.; Li, L. Zeolite-Encaged Isolated Platinum Ions Enable Heterolytic Dihydrogen Activation and Selective Hydrogenations. *J. Am. Chem. Soc.* **2021**, *143*, 20898−20906.

(7) Jin, Y.; Wang, P.; Mao, X.; Liu, S.; Li, L.; Wang, L.; Shao, Q.; Xu, Y.; Huang, X. A Top-Down Strategy to Realize Surface Reconstruction of Small-Sized Platinum-Based Nanoparticles for Selective Hydrogenation. *Angew. Chem., Int. Ed.* **2021**, *60*, 17430−17434.

(8) Lv, H.; Qin, H.; Ariga, K.; Yamauchi, Y.; Liu, B. A General Concurrent Template Strategy for Ordered Mesoporous Intermetallic Nanoparticles with Controllable Catalytic Performance. *Angew. Chem., Int. Ed.* **2022**, *61*, e202116179.

(9) Sorribes, I.; Liu, L.; Corma, A. Nanolayered Co-Mo-S Catalysts for the Chemoselective Hydrogenation of Nitroarenes. *Acs Catal.* **2017**, *7*, 2698−2708.

(10) Gao, R.; Pan, L.; Wang, H.; Zhang, X.; Wang, L.; Zou, J.-J. Ultradispersed Nickel Phosphide on Phosphorus-Doped Carbon with Tailored d-Band Center for Efficient and Chemoselective Hydrogenation of Nitroarenes. *ACS Catal.* **2018**, *8*, 8420−8429.

(11) Han, A.; Zhang, J.; Sun, W.; Chen, W.; Zhang, S.; Han, Y.; Feng, Q.; Zheng, L.; Gu, L.; Chen, C.; Peng, Q.; Wang, D.; Li, Y. Isolating contiguous Pt atoms and forming Pt-Zn intermetallic nanoparticles to regulate selectivity in 4-nitrophenylacetylene hydrogenation. *Nat. Commun.* **2019**, *10*, 3787.

(12) Xie, C.; Niu, Z.; Kim, D.; Li, M.; Yang, P. Surface and Interface Control in Nanoparticle Catalysis. *Chem. Rev.* **2020**, *120*, 1184−1249.

(13) Gao, C.; Lyu, F.; Yin, Y. Encapsulated Metal Nanoparticles for Catalysis. *Chem. Rev.* **2021**, *121*, 834−881.

(14) Li, Z.; Xu, Q. Metal-Nanoparticle-Catalyzed Hydrogen Generation from Formic Acid. *Acc. Chem. Res.* **2017**, *50*, 1449−1458.

(15) Zhang, Y.; Cui, X.; Shi, F.; Deng, Y. Nano-gold Catalysis in Fine Chemical Synthesis. *Chem. Rev.* **2012**, *112*, 2467−505.
(16) Huang, Y.; Zhao, M.; Han, S.; Lai, Z.; Yang, J.; Tan, C.; Ma, Q.; Lu, Q.; Chen, J.; Zhang, X.; Zhang, Z.; Li, B.; Chen, B.; Zong, Y.; Zhang, H. Growth of Au Nanoparticles on 2D Metalloporphyrinic Metal-Organic Framework Nanosheets Used as Biomimetic Catalysts for Cascade Reactions. *Adv. Mater.* **2017**, *29*, 1700102.
(17) Li, J.; Zeng, H. Size Tuning, Functionalization, and Reactivation of Au in TiO_2 Nanoreactors. *Angew. Chem., Int. Ed.* **2005**, *44*, 4342−4345.
(18) Chen, Y.; Zhu, Q. L.; Tsumori, N.; Xu, Q. Immobilizing Highly Catalytically Active Noble Metal Nanoparticles on Reduced Graphene Oxide: a Non-noble Metal Sacrificial Approach. *J. Am. Chem. Soc.* **2015**, *137*, 106−109.
(19) Liu, L.; Asano, T.; Nakagawa, Y.; Tamura, M.; Okumura, K.; Tomishige, K. Selective Hydrogenolysis of Glycerol to 1,3-Propanediol over Rhenium-Oxide-Modified Iridium Nanoparticles Coating Rutile Titania Support NP. *ACS Catal.* **2019**, *9*, 10913−10930.
(20) Huang, H.; Jia, H.; Liu, Z.; Gao, P.; Zhao, J.; Luo, Z.; Yang, J.; Zeng, J. Understanding of Strain Effects in the Electrochemical Reduction of CO_2: Using Pd Nanostructures as an Ideal Platform. *Angew. Chem.* **2017**, *129*, 3648−3652.
(21) Aijaz, A.; Karkamkar, A.; Choi, Y. J.; Tsumori, N.; Ronnebro, E.; Autrey, T.; Shioyama, H.; Xu, Q. Immobilizing Highly Catalytically Active Pt Nanoparticles inside the Pores of Metal-organic Framework: a Double Solvents Approach. *J. Am. Chem. Soc.* **2012**, *134*, 13926−13929.
(22) Liu, H.; Chang, L.; Bai, C.; Chen, L.; Luque, R.; Li, Y. Controllable Encapsulation of "Clean" Metal Clusters within MOFs through Kinetic Modulation: Towards Advanced Heterogeneous Nanocatalysts. *Angew. Chem., Int. Ed.* **2016**, *55*, 5019−5023.
(23) Zhan, G.; Li, P.; Zeng, H. Architectural Designs and Synthetic Strategies of Advanced Nanocatalysts. *Adv. Mater.* **2018**, *30*, 1802094.
(24) Zhu, Q.-L.; Xu, Q. Immobilization of Ultrafine Metal Nanoparticles to High-Surface-Area Materials and Their Catalytic Applications. *Chem.* **2016**, *1*, 220−245.
(25) Goswami, S.; Noh, H.; Redfern, L. R.; Otake, K.-i.; Kung, C.-W.; Cui, Y.; Chapman, K. W.; Farha, O. K.; Hupp, J. T. Pore-Templated Growth of Catalytically Active Gold Nanoparticles within a Metal-Organic Framework. *Chem. Mater.* **2019**, *31*, 1485−1490.
(26) Zhu, Q. L.; Li, J.; Xu, Q. Immobilizing Metal Nanoparticles to Metal-Organic Frameworks with Size and Location Control for Optimizing Catalytic Performance. *J. Am. Chem. Soc.* **2013**, *135*, 10210−10213.
(27) Furukawa, H.; Cordova, K. E.; O'Keeffe, M.; Yaghi, O. M. The Chemistry and Applications of Metal-Organic Frameworks. *Science* **2013**, *341*, 1230444.
(28) Zhao, M.; Yuan, K.; Wang, Y.; Li, G.; Guo, J.; Gu, L.; Hu, W.; Zhao, H.; Tang, Z. Metal-Organic Frameworks as Selectivity Regulators for Hydrogenation Reactions. *Nature* **2016**, *539*, 76−80.
(29) Parker, S. T.; Smith, A.; Forse, A. C.; Liao, W.-C.; Brown-Altvater, F.; Siegelman, R. L.; Kim, E. J.; Zill, N. A.; Zhang, W.; Neaton, J. B.; Reimer, J. A.; Long, J. R. Evaluation of the Stability of Diamine-Appended Mg_2(dobpdc) Frameworks to Sulfur Dioxide. *J. Am. Chem. Soc.* **2022**, *144*, 19849−19860.
(30) Kirchon, A.; Feng, L.; Drake, H. F.; Joseph, E. A.; Zhou, H.-C. From Fundamentals to Applications: a Toolbox for Robust and Multifunctional MOF materials. *Chem. Soc. Rev.* **2018**, *47*, 8611−8638.
(31) Ma, D.; Li, P.; Duan, X.; Li, J.; Shao, P.; Lang, Z.; Bao, L.; Zhang, Y.; Lin, Z.; Wang, B. A Hydrolytically Stable Vanadium(IV) Metal-Organic Framework with Photocatalytic Bacteriostatic Activity for Autonomous Indoor Humidity Control. *Angew. Chem., Int. Ed.* **2020**, *59*, 3905−3909.
(32) Li, B.; Wen, H.; Cui, Y.; Zhou, W.; Qian, G. D.; Chen, B. L. Emerging Multifunctional Metal-Organic Framework Materials. *Adv. Mater.* **2016**, *28*, 8819−8860.
(33) He, J.; Li, N.; Li, Z.-G.; Zhong, M.; Fu, Z.-X.; Liu, M.; Yin, J.-C.; Shen, Z.; Li, W.; Zhang, J.; Chang, Z.; Bu, X.-H. Strategic Defect Engineering of Metal-Organic Frameworks for Optimizing the Fabrication of Single-Atom Catalysts. *Adv. Funct. Mater.* **2021**, *31*, 2103597.
(34) Yi, J.; Si, D.; Xie, R.; Yin, Q.; Zhang, M.; Wu, Q.; Chai, G.; Huang, Y.; Cao, R. Conductive Two-Dimensional Phthalocyanine-based Metal-Organic Framework Nanosheets for Efficient Electroreduction of CO_2. *Angew. Chem., Int. Ed.* **2021**, *60*, 17108−17114.
(35) Shi, Y.; Zhang, W.; Abrahams, B.; Braunstein, P.; Lang, J. P. Fabrication of New Photoactuators: Macroscopic Photomechanical Responses of Metal-Organic Frameworks to Irradiation by UV light. *Angew. Chem., Int. Ed.* **2019**, *58*, 9453−9458.
(36) Medishetty, R.; Nalla, V.; Nemec, L.; Henke, S.; Mayer, D.; Sun, H.; Reuter, K.; Fischer, R. A. A New Class of Lasing Materials: Intrinsic Stimulated Emission from Nonlinear Optically Active Metal-Organic Frameworks. *Adv. Mater.* **2017**, *29*, 1605637.
(37) Lu, G.; Li, S.; Guo, Z.; Farha, O. K.; Hauser, B. G.; Qi, X.; Wang, Y.; Wang, X.; Han, S.; Liu, X.; DuChene, J. S.; Zhang, H.; Zhang, Q.; Chen, X.; Ma, J.; Loo, S. C. J.; Wei, W. D.; Yang, Y.; Hupp, J. T.; Huo, F. Imparting Functionality to a Metal-organic Framework Material by Controlled Nanoparticle Encapsulation. *Nat. Chem.* **2012**, *4*, 310−316.
(38) Yang, Q.; Liu, W.; Wang, B.; Zhang, W.; Zeng, X.; Zhang, C.; Qin, Y.; Sun, X.; Wu, T.; Liu, J.; Huo, F.; Lu, J. Regulating the Spatial Distribution of Metal Nanoparticles within Metal-Organic Frameworks to Enhance Catalytic Efficiency. *Nat. Commun.* **2017**, *8*, 14429.
(39) Guo, J.; Wan, Y.; Zhu, Y.; Zhao, M.; Tang, Z. Advanced Photocatalysts based on Metal Nanoparticle/Metal-Organic Framework Composites. *Nano Research* **2021**, *14*, 2037−2052.
(40) Moon, H. R.; Lim, D.-W.; Suh, M. P. Fabrication of Metal Nanoparticles in Metal-Organic Frameworks. *Chem. Soc. Rev.* **2013**, *42*, 1807−1824.
(41) Lim, D.-W.; Kitagawa, H. Proton Transport in Metal-Organic Frameworks. *Chem. Rev.* **2020**, *120*, 8416−8467.
(42) Zhan, G.; Zeng, H. Integrated Nanocatalysts with Mesoporous Silica/Silicate and Microporous MOF Materials. *Coord. Chem. Rev.* **2016**, *320*, 181−192.
(43) Wang, H.; Wang, L.; Lin, D.; Feng, X.; Niu, Y.; Zhang, B.; Xiao, F.-S. Strong Metal-Support Interactions on Gold Nanoparticle Catalysts achieved through Le Chatelier's Principle. *Nat. Catal.* **2021**, *4*, 418−424.
(44) van Deelen, T. W.; Hernández Mejía, C.; de Jong, K. P. Control of Metal-Support Interactions in Heterogeneous Catalysts to Enhance Activity and Selectivity. *Nat. Catal.* **2019**, *2*, 955−970.
(45) Trickett, C. A.; Osborn Popp, T. M.; Su, J.; Yan, C.; Weisberg, J.; Huq, A.; Urban, P.; Jiang, J.; Kalmutzki, M. J.; Liu, Q.; Baek, J.; Head-Gordon, M. P.; Somorjai, G. A.; Reimer, J. A.; Yaghi, O. M. Identification of the Strong Brønsted Acid Site in a Metal-Organic Framework Solid Acid Catalyst. *Nat. Chem.* **2019**, *11*, 170−176.
(46) Yang, J.; Li, W. H.; Tan, S.; Xu, K.; Wang, Y.; Wang, D.; Li, Y. The Electronic Metal-Support Interaction Directing the Design of Single Atomic Site Catalysts: Achieving High Efficiency Towards Hydrogen Evolution. *Angew. Chem., Int. Ed.* **2021**, *60*, 19085−19091.
(47) Jiang, Z.; Tian, M.; Jing, M.; Chai, S.; Jian, Y.; Chen, C.; Douthwaite, M.; Zheng, L.; Ma, M.; Song, W.; Liu, J.; Yu, J.; He, C. Modulating the Electronic Metal-Support Interactions in Single-Atom Pt_1 Catalyst for Boosting Acetone Oxidation. *Angew. Chem., Int. Ed.* **2022**, *61*, e202200763.
(48) Zhou, C.; Wu, K.; Huang, H.; Cao, C.-F.; Luo, Y.; Chen, C.-Q.; Lin, L.; Au, C.; Jiang, L. Spatial Confinement of Electron-Rich Ni Nanoparticles for Efficient Ammonia Decomposition to Hydrogen Production. *ACS Catal.* **2021**, *11*, 10345−10350.
(49) Wang, C.; An, B.; Lin, W. Metal-Organic Frameworks in Solid-Gas Phase Catalysis. *ACS Catal.* **2019**, *9*, 130−146.
(50) Ji, P.; Manna, K.; Lin, Z.; Urban, A.; Greene, F.; Lan, G.; Lin, W. Single-Site Cobalt Catalysts at New $Zr_8(\mu_2\text{-}O)_8(\mu_2\text{-}OH)_4$ Metal-Organic Framework Nodes for Highly Active Hydrogenation of Alkenes, Imines, Carbonyls, and Heterocycles. *J. Am. Chem. Soc.* **2016**, *138*, 12234−12242.

https://doi.org/10.1021/jacs.2c12590
J. Am. Chem. Soc. 2023, 145, 4659−4666

(51) Feng, L.; Wang, K.-Y.; Lv, X.-L.; Powell, J. A.; Yan, T.-H.; Willman, J.; Zhou, H.-C. Imprinted Apportionment of Functional Groups in Multivariate Metal-Organic Frameworks. *J. Am. Chem. Soc.* **2019**, *141*, 14524−14529.
(52) Wang, G.; He, C. T.; Huang, R.; Mao, J.; Wang, D.; Li, Y. Photoinduction of Cu Single Atoms Decorated on UiO-66-NH_2 for Enhanced Photocatalytic Reduction of CO_2 to Liquid Fuels. *J. Am. Chem. Soc.* **2020**, *142*, 19339−19345.
(53) Feng, L.; Day, G. S.; Wang, K.-Y.; Yuan, S.; Zhou, H.-C. Strategies for Pore Engineering in Zirconium Metal-Organic Frameworks. *Chem.* **2020**, *6*, 2902−2923.
(54) Isaka, Y.; Kawase, Y.; Kuwahara, Y.; Mori, K.; Yamashita, H. Two-Phase System Utilizing Hydrophobic Metal-Organic Frameworks (MOFs) for Photocatalytic Synthesis of Hydrogen Peroxide. *Angew. Chem., Int. Ed.* **2019**, *58*, 5402−5406.
(55) Xu, M.; Li, D.; Sun, K.; Jiao, L.; Xie, C.; Ding, C.; Jiang, H.-L. Interfacial Microenvironment Modulation Boosting Electron Transfer between Metal Nanoparticles and MOFs for Enhanced Photocatalysis. *Angew. Chem., Int. Ed.* **2021**, *60*, 16372−16376.
(56) Yen, C. I.; Liu, S. M.; Lo, W. S.; Wu, J. W.; Liu, Y. H.; Chein, R. J.; Yang, R.; Wu, K. C.; Hwu, J. R.; Ma, N.; Shieh, F. K. Cytotoxicity of Postmodified Zeolitic Imidazolate Framework-90 (ZIF-90) Nanocrystals: Correlation between Functionality and Toxicity. *Chem.—Eur. J.* **2016**, *22*, 2925−2929.
(57) Yan, L.; Brouzgou, A.; Meng, Y.; Xiao, M.; Tsiakaras, P.; Song, S. Efficient and Poison-tolerant PdxAuy/C Binary Electrocatalysts for Glucose Electrooxidation in Alkaline Medium. *Appl. Catal. B: Environ.* **2014**, *150−151*, 268−274.
(58) Yan, R.; Zhao, Y.; Yang, H.; Kang, X.-J.; Wang, C.; Wen, L.-L.; Lu, Z.-D. Ultrasmall Au Nanoparticles Embedded in 2D Mixed-Ligand Metal-Organic Framework Nanosheets Exhibiting Highly Efficient and Size-Selective Catalysis. *Adv. Funct. Mater.* **2018**, *28*, 1802021.
(59) Zhan, G.; Fan, L.; Zhao, F.; Huang, Z.; Chen, B.; Yang, X.; Zhou, S.-f. Fabrication of Ultrathin 2D Cu-BDC Nanosheets and the Derived Integrated MOF Nanocomposites. *Adv. Funct. Mater.* **2019**, *29*, 1806720.
(60) Zhao, J.-X.; Chen, C.-Q.; Xing, C.-H.; Jiao, Z.-F.; Yu, M.-T.; Mei, B.-B.; Yang, J.; Zhang, B.-Y.; Jiang, Z.; Qin, Y. Selectivity Regulation in Au-Catalyzed Nitroaromatic Hydrogenation by Anchoring Single-Site Metal Oxide Promoters. *Acs Catal.* **2020**, *10*, 2837−2844.
(61) Morris, W.; Doonan, C.; Furukawa, H.; Banerjee, R.; Yaghi, O. Crystals as Molecules: Postsynthesis Covalent Functionalization of Zeolitic Imidazolate Frameworks. *J. Am. Chem. Soc.* **2008**, *130*, 12626−12627.
(62) Liu, Q.; Yang, X.; Li, L.; Miao, S.; Li, Y.; Li, Y.; Wang, X.; Huang, Y.; Zhang, T. Direct Catalytic Hydrogenation of CO_2 to Formate over a Schiff-Base-Mediated Gold Nanocatalyst. *Nat. Commun.* **2017**, *8*, 1407.
(63) Wang, X.; Wang, W.; Qiao, M.; Wu, G.; Chen, W.; Yuan, T.; Xu, Q.; Chen, M.; Zhang, Y.; Wang, X.; Wang, J.; Ge, J.; Hong, X.; Li, Y.; Wu, Y.; Li, Y. Atomically Dispersed Au_1 Catalyst towards Efficient Electrochemical Synthesis of mmonia. *Science Bulletin* **2018**, *63*, 1246−1253.
(64) Wang, L.; Zhu, C.; Xu, M.; Zhao, C.; Gu, J.; Cao, L.; Zhang, X.; Sun, Z.; Wei, S.; Zhou, W.; Li, W. X.; Lu, J. Boosting Activity and Stability of Metal Single-Atom Catalysts *via* Regulation of Coordination Number and Local Composition. *J. Am. Chem. Soc.* **2021**, *143*, 18854−18858.
(65) Yang, Y.; Li, F.; Chen, J.; Fan, J.; Xiang, Q. Single Au Atoms Anchored on Amino-Group-Enriched Graphitic Carbon Nitride for Photocatalytic CO_2 Reduction. *ChemSusChem* **2020**, *13*, 1979−1985.
(66) Chen, Z.; Zhang, Q.; Chen, W.; Dong, J.; Yao, H.; Zhang, X.; Tong, X.; Wang, D.; Peng, Q.; Chen, C.; He, W.; Li, Y. Single-Site Au(I) Catalyst for Silane Oxidation with Water. *Adv. Mater.* **2018**, *30*, 1704720.
(67) Jin, H.; Li, P.; Cui, P.; Shi, J.; Zhou, W.; Yu, X.; Song, W.; Cao, C. Unprecedentedly High Activity and Selectivity for Hydrogenation of Nitroarenes with Single Atomic Co_1-N_3P_1 Sites. *Nat. Commun.* **2022**, *13*, 723.
(68) Corma, A.; Serna, P.; Concepción, P.; Calvino, J. J. Transforming Nonselective into Chemoselective Metal Catalysts for the Hydrogenation of Substituted Nitroaromatics. *J. Am. Chem. Soc.* **2008**, *130*, 8748−8753.
(69) Chen, P.; Yang, F.; Kostka, A.; Xia, W. Interaction of Cobalt Nanoparticles with Oxygen- and Nitrogen-Functionalized Carbon Nanotubes and Impact on Nitrobenzene Hydrogenation Catalysis. *ACS Catal.* **2014**, *4*, 1478−1486.
(70) Wang, Y.; Tian, H.; Li, H.; Deng, X.; Zhang, Q.; Ai, Y.; Sun, Z.; Wang, Y.; Liu, L.; Hu, Z.-N.; Zhang, X.; Guo, R.; Xu, W.; Liang, Q.; Sun, H.-B. Encapsulating Electron-Rich Pd NPs with Lewis Acidic MOF: Reconciling the Electron-Preference Conflict of the Catalyst for Cascade Condensation *via* Nitro Reduction. *Acs Appl. Mater. Inter.* **2022**, *14*, 7949−7961.
(71) Yang, Q.; Jiang, H.-L. Oxidation or Reduction State of Au Stabilized by an MOF: Active Site Identification for the Three-Component Coupling Reaction. *Small Methods* **2018**, *2*, 1800216.
(72) Zhang, X.; Shi, H.; Xu, B. Comparative study of Au/ZrO_2 catalysts in CO oxidation and 1,3-butadiene hydrogenation. *Catal. Today.* **2007**, *122*, 330−337.

https://doi.org/10.1021/jacs.2c12590
J. Am. Chem. Soc. 2023, 145, 4659−4666